Regenerative Therapy 27 (2024) 48–62

Contents lists available at ScienceDirect

Regenerative Therapy

journal homepage: http://www.elsevier.com/locate/reth

Original Article

Biological characteristics of Muse cells derived from MenSCs and their application in acute liver injury and intracerebral hemorrhage diseases

Han Li [a], Jinghui Wei [a], Mingzhi Li [a], Yaoqiang Li [a], Tong Zhang [a], Jialu Tian [a], Xuejia Liu [a], Kangjia Li [a], Juntang Lin [b, *]

[a] Stem Cells and Biotherapy Engineering Research Center of Henan, National Joint Engineering Laboratory of Stem Cells and Biotherapy, School of Life Science and Technology, Xinxiang Medical University, Xinxiang 453003, China
[b] Henan Joint International Research Laboratory of Stem Cell Medicine, School of Medical Engineering, Xinxiang Medical University, Xinxiang 453003, China

ARTICLE INFO

Article history:
Received 28 November 2023
Received in revised form
16 February 2024
Accepted 3 March 2024

Keywords:
MenSCs
Muse cell
Acute liver injury
Intracerebral hemorrhage
Cell transplantation
Regenerative medicine

ABSTRACT

The increasing interest in multilineage differentiating stress-enduring (Muse) cells within the field of regenerative medicine is attributed to their exceptional homing capabilities, prolonged viability in adverse conditions, and enhanced three-germ-layer differentiate ability, surpassing their parent mesenchymal stem cells. Given their abundant sources, non-invasive collection procedure, and periodic availability, human menstrual blood-derived endometrium stem cells (MenSCs) have been extensively investigated as a potential resource for stem cell-based therapies. However, there is no established modality to isolate Muse cells from MenSCs and disparity in gene expression profiles between Muse cells and MenSCs remain unknown. In this study, Muse cells were isolated from MenSCs by long-time trypsin incubation method. Muse cells expressed pluripotency markers and could realize multilineage differentiation *in vitro*. Compared with MenSCs, Muse cells showed enhanced homing ability and superior therapeutic efficacy in animal models of acute liver injury (ALI) and intracerebral hemorrhage (ICH). Furthermore, the RNA-seq analysis offers insights into the mechanism underlying the disparity in trypsin resistance and migration ability between Muse and MenSCs cells. This research offers a significant foundation for further exploration of cell-based therapies using MenSCs-derived Muse cells in the context of various human diseases, highlighting their promising application in the field of regenerative medicine.

1. Introduction

Mesenchymal stem cells (MSCs) have attracted public attention in regenerative medicine field due to their regenerative ability, immunomodulatory ability, and limited ethical concerns [1]. Most importantly, nearly 500 MSCs clinical trial studies (ClinicalTrials.gov) have been completed worldwide. There were no any cases of tumorigenesis after MSCs transplantation. MSCs have made major breakthroughs in cardiovascular disease, neurological diseases, pulmonary dysfunctions, metabolic/endocrine-related diseases, reproductive disorders, etc. [2]. However, several shortcomings of MSCs limit their therapeutic outcome in regenerative medicine. Although MSCs are capable of multidirectional differentiation, the differentiation potential of across germ layers is very limited [3,4]. With intravenous administration, most MSCs would be trapped in lung and only minority of MSCs can migrate to injury sites to repair damaged tissues [5]. Additionally, MSCs are usually undetectable one month after transplantation because of their removal by macrophages [6]. Indeed, the highly inflammatory and oxidative stress environment in the injury site is hostile to the survival of MSCs, especially in the acute and subacute phases of diseases [7].

Multilineage-differentiating stress-enduring (Muse) cells were first identified in bone marrow-derived mesenchymal stem cells (BM-MSCs) in 2010 [8,9]. Over the past decade, Muse cells have been successively identified in peripheral blood [10], umbilical cord [11], adipose tissue [12–14], and dermal fibroblasts [9,15]. Muse cells were reported to express both MSCs marker CD105 and SSEA3 specifically [8].

* Corresponding author.
E-mail address: linjtlin@126.com (J. Lin).
Peer review under responsibility of the Japanese Society for Regenerative Medicine.

https://doi.org/10.1016/j.reth.2024.03.003

Compared with MSCs, Muse cells are pluripotent, which could differentiate into three-germ-layer cells and are more tolerant to harsh environments [12]. Additionally, Muse cells can escape from the entrapment of lung capillaries and preferentially home to the injury sites [16]. Since Muse cell could compensate the shortcomings of MSCs, it represents a promising therapeutic tool to improve the treatment outcome of various diseases.

Menstrual blood-derived endometrium stem cells (MenSCs) came to the attention of public in 2007 [17,18]. Compared to other sources of MSCs, menstrual blood sample could be collected periodically and non-invasively [19]. According to our previous study, 30–50 ml menstrual blood could be collected during menstruation and 5 ml sample could expand 100 million passage 3 MSCs, which is sufficient for scientific research and clinical treatment [19]. However, the system of isolation and culture of Muse cells from MenSCs has not been established.

Consequently, this study aimed to develop a technique for isolating Muse cells from MenSCs and investigate their biological attributes. Subsequently, the migratory capacity and therapeutic efficacy of Muse cells and MenSCs were compared in models of intracerebral hemorrhage and acute liver injury. Lastly, RNA-seq and bioinformatic analyses were conducted to elucidate the disparities in gene expression between Muse cells and MenSCs, thereby providing insights into the underlying mechanisms governing the distinct characteristics exhibited by these cell types.

2. Methods

2.1. Ethics

This study was approved by the Ethics Committee of Xinxiang Medical University (approval number: XYLL-20220137). All animal procedures were performed in agreement with the National Institutes of Health guidelines and in compliance with the ARRIVE guidelines 2.0. Written informed consent was obtained from all menstrual blood donors involved in this study.

2.2. Animals and experimental design

Wild male SD rats (220–250 g), wild male BALB/c mice (20–24 g) and NOD/SCID male mice (20–24 g) were purchased from Beijing Vital River Laboratory Animal Technology Co., Ltd. (Beijing, China). Wild male SD rats were employed for intracerebral hemorrhage related experiments. Wild male BALB/c mice were employed for acute liver injury related experiments. NOD/SCID male mice were employed only for testis tumorigenicity research. Animals were maintained under standard laboratory conditions with 12 h light/dark cycle, 23 ± 2 °C, and 45–60% humidity. They were watered and fed ad libitum. After adapting to the new environment for 5–7 days, they were used for model construction or cell transplantation. All the experimental conditions were performed in a within-subject randomized-order design. The operator and designer were blinded to each other.

2.3. Isolation and immunophenotyping of MenSCs

MenSCs were isolated and cultured as previously described [19]. According to the minimal criteria for defining MSCs given by International Society for Cellular Therapy [20], passage 3 MenSCs were underwent immunophenotyping identification with CD73-APC, CD90-FITC, CD105-PerCP-Cy5.5, CD11b-PE, CD34-PE, CD45-PE, HLA-DR-PE, CD146 and PDGF-β by flow cytometry. All antibodies were purchased from BD Pharmingen (San Jose, USA) except for CD146 and PDGF-β, which were purchased from Proteintech (Wuhan, China). Three independent experiments were performed.

Briefly, cell concentration was adjusted to 5×10^5/100 μL. After blocking with 3% BSA for 15 min on ice, 1 μL CD73-APC, CD90-FITC, CD105-PerCP-Cy5.5, CD11b-PE, CD34-PE, CD45-PE, HLA-DR-PE and their relative isotype control antibodies were incubated with cells on ice for 20 min in dark. Primary antibodies CD146 (1 μL) and PDGF-β (0.25 μL) were incubated with cells for 20 min, and then incubated with Alexa488 conjugated goat anti-mouse (A28175, Introvegen) and goat anti-rabbit (A11034, Introvegen) secondary antibodies for 20 min, respectively. Cells only incubated with relative secondary antibodies were treated as control group. After washed once to remove uncombined antibodies, cells were resuspended in 500 μL blocking buffer. Data (10,000 events) were collected using a FACS Calibur (BD Biosciences, CA, USA) and analyzed using FlowJo version10 software.

2.4. Trypsin treatment and cell viability detection

MenSCs were normally detached by 0.25% trypsin solution (25200072, Gibco) and washed twice by PBS to remove culture medium and serum. Then, MenSCs were incubated with 0.25% trypsin as a concentration of 1×10^5 cells/mL at 37 °C for 8 h, 16 h, and 24 h, respectively. Then cells were stained by trypan blue and the number of alive cells and dead cells was counted by a fully-automated cell counter. Three independent experiments were performed.

2.5. Preparation of Muse-enriched cells (MECs)

MenSCs of 4–6 passage were used to prepare Muse cells. Muse cells were enriched by exposing MenSCs with long-term trypsin (LTT) incubation. Specifically, MenSCs were suspended in 0.25% trypsin, and incubated at 37 °C for 8 h. After centrifuged at 1500 rpm for 5 min, cells were re-suspended in DMEM completed medium and seeded in 1% aqueous gelatin-coated culture dishes as a density of 8×10^4/mL. The next day, the medium was changed to remove non-adherent cells. The attached cells were termed Muse-enriched cells (MECs) and were used for following studies.

2.6. Preparation of M-clusters and Muse cells

MECs were suspended in DMEM high glucose medium (Corning, NY, USA) supplemented with 0.9% MethoCult (H4100, StemCell Technologies Inc.), 10% FBS (Gibco, Grand Island, NY), and 1% penicillin/streptomycin (Gibco). Then, the mixture was seeded in poly-HEMA (P3932, Sigma–Aldrich, Saint Louis, MO, USA) pretreated 96-well cell culture plate by limited dilution method, 70 μL for each well. Wells containing 1–3 cells were chosen for following studies. 30 μL complete DMEM medium containing 10% FBS and 1% penicillin/streptomycin was added every 3 days. After 7–10 days, single Muse cell will grow to a Muse-cluster (M-cluster), while non-Muse cell cannot generate a cluster. The generated M-clusters were used for immunocytochemistry, ALP staining and tumorigenicity assays. To prepare adherent Muse cells, M-clusters were collected by centrifuging at 1500 rpm for 5 min, resuspended in complete medium, and then placed in cell culture dishes for normal adherent culture. When reaching 70%–80% confluency, cells were used for multilineage differentiation, immunocytochemistry, migration assay *in vitro* and cell transplantation *in vivo*.

2.7. Multilineage differentiation assay in vitro

Adipogenesis, osteogenesis, and chondrogenesis differentiations of Muse cells were performed following the protocols described in our previously published paper [19]. Three independent experiments were performed.

As to neural cell induction, Muse cells were adjusted to 4.8×10^4 cells/mL with neural precursor cell induction medium and seeded in poly-HEMA-treated 48-well plates. 1 mL neural precursor cell induction medium contained 957 μL Neurobasal medium, 20 μL B27 supplement (50×), 10 μL L-glutamin (100×), 1.5 μL bFGF (20 μg/mL), 1.5 μL EGF (20 μg/mL), and 10 μL of penicillin/streptomycin (100×). Half of the medium was changed every 3 days, and after 7 days of induction, specific aggregates of cells were formed, termed neurospheres. A portion of the neurospheres was subjected to immunofluorescence staining for neural precursor cell markers Nestin and DCX. The remained neurospheres were placed in gelatin-coated 48-well plates for further differentiation induction. 1 mL induction medium contained 977.725 μL α-MEM medium, 20 μL FBS, 1 μL BDNF (25 μg/mL) and 1.275 μL bFGF (20 μg/mL). Half of the medium was replaced every three days, and immunofluorescence staining for mature neural or gliocyte markers including MAP-2, Tuj-1, GAP-43, and S100β was performed after 10–14 days of induction. Three independent experiments were performed.

2.8. Immunocytochemistry

M-clusters were generated by limited dilution of MECs in suspension culture condition, which was detailed in "Preparation of M-clusters and Muse cells" section. Muse cells were achieved by adherent culture of M-clusters. For CD105 and SSEA3 double staining, M-clusters and attached Muse cells were fixed with 4% paraformaldehyde (PFA) for 15 min, permeabilized with 0.1% Triton X-100 for 5 min, and blocked with 5% BSA (A1933, Sigma) for 1 h at room temperature. Afterwards, cells were incubated with primary antibody CD105 (10862-1-AP, Proteintech) overnight at 4 °C, followed by incubation with Cy3-conjugated secondary antibody (A10520, Invitrogen, Carlsbad, CA, USA) for 2 h at room temperature. After washing with PBS for 3 times, cells were incubated with SSEA3 primary antibody (330302, Biolegend, CA, USA) overnight at 4 °C, followed by incubation with FITC-conjugated secondary antibody (112-095-075, Jackson Immunoresearch, Westgrove, PA, US) for 2 h at room temperature.

For pluripotent markers detection of M-clusters, after regular fixation, membrane permeabilization, and blocking, cells were incubated with primary antibodies against Nanog (14295, Proteintech), Oct4 (60242, Proteintech), and Sox2 (66411, Proteintech) overnight at 4 °C.

To evaluate the neurogenic induction differentiation ability of Muse cells, neurospheres generated in the first step of neurogenic induction differentiation (Muse-NPC sphere) were aspirated and incubated with Nestin (19483-1-AP, Proteintech) and DCX antibody (ab18723, abcam, MA, USA) overnight at 4 °C. MAP2 (ab32454, abcam), Tuj1 (T3952, Sigma), GAP43 (sc-33705, Santa Cruz Biotechnology, Santa Cruz, CA), and S100β (15146-1-AP, Proteintech) were used to detect the mature neurons and glia cells generated in the second step. After incubated with the corresponding secondary antibody for 2 h, nuclei were counterstained with DAPI. Images were photographed using a confocal laser scanning microscope (Leica, DMI3000B, Germany). Three independent experiments were performed.

2.9. ALP staining of M-clusters

ALP staining buffer was prepared by dissolving 0.6 g of Tris base and 0.292 g of NaCl in 50 mL ultrapure water (pH = 9.5). ALP staining solution was freshly prepared by mixing 35 μL of 50 mg/mL BCIP and 45 μL of 25 mg/mL NBT (N6547, Invitrogen) in 10 mL staining buffer. Matured M-clusters were transferred to 48-well plate and allowed to attach for 8 h. Then clusters were fixed with 4% PFA at 4 °C for 15 min. After washed 3 times with saline, clusters were incubated with ALP staining solution for 30–45 min in the dark at 37 °C. Then, PBS was applied to stop the staining process. Imaging was performed using a conventional light microscope (BX50, Olympus). Induced pluripotent stem cells (iPSCs) were used as positive control. Three independent experiments were performed.

2.10. Acute liver injury mouse model construction

The mice were randomly divided into two groups by lottery method: Sham group ($n = 6$) and ALI group ($n = 18$). Briefly, CCl_4 (1601168, Merk, Darmstadt, Germany) was dissolved in olive oil at a ratio of 1:10 to make a working solution. ALI group mice were intraperitoneally (i.p.) injected with a single dose of 1.5 mL/kg CCl_4 working solution, while control group mice were i.p. injected with equal dose of olive oil.

2.11. Intracerebral hemorrhage rat model construction

The rats were randomly divided into two groups by lottery method: Sham group ($n = 6$) and ICH group ($n = 18$). Rats were anesthetized with 4% isoflurane using an anesthetic gas machine and fixed on a brain stereoscopic injection equipment. 2.5% isoflurane and 1 L/min oxygen were used for continuous anesthesia during surgery. ICH model was constructed by unilaterally stereotactic injection of collagenase VII (0.2 U in 1 μL sterile saline, C0773; Sigma–Aldrich) to striatum region according to the Paxinos and Watson brain atlas [21]. The injection coordinates related to bregma was M/L = +0.5 mm, A/P = −3.0 mm, D/V = −5.87 mm. Rats of Sham group were injected with 1 μL sterile saline. After injection, the needle was left in place for an additional 10 min to minimize backflow.

2.12. Serum collection

After ICH surgery for 72 h and CCl_4 injection for 24 h, blood samples were collected from the orbital venous plexus of rats or mice using capillary needles. After coagulation stratification for 2 h at room temperature, samples were centrifugated at 3000 rpm for 10 min. The upper layer serum was collected and stored at −80 °C for cell migration assay *in vitro*.

2.13. Cell migration assay in vitro

The migration assay was performed using 24-well transwell chambers (8.0 μm, Corning Inc.). The lower chamber was filled with 675 μL DMEM high glucose medium and 75 μL serum from healthy mice, ALI mice, healthy rats or ICH rats ($n = 3$ per group). The upper chamber contained 2.5×10^4 Muse cells or MenSCs, which had been starved for 24 h to remove the effects of serum. After co-culture for 22 h, the unmigrated cells were carefully wiped off with a wet cotton rod. Then, the chamber was fixed by methanol and stained by Giemsa solution at room temperature for 15–30 min. The chamber was rinsed gently with clean water and put in the fume hood to dry. Photographs were taken using an inverted bright-field microscope (Olympus IX50) at ×400 magnification. 16 randomly selected fields were counted and analyzed for each group.

2.14. Cell transplantation

1,1-Dioctadecyl-3,3,3,3-tetramethylindocarbocyanine perchlorate (DiL) (Sigma) was used to label Muse cells and MenSCs. Briefly, after culture with DiL (2.5 μg/mL, Cat#468495, Sigma) for 12 h in incubator, cells were detached and washed 3 times with PBS.

Rats were divided into four groups by lottery method: Sham ($n = 6$), ICH + PBS ($n = 6$), ICH + MenSCs ($n = 6$), and ICH + Muse ($n = 6$). For ICH rat treatment, 5×10^5 MenSCs (ICH + MenSCs group) or Muse cells (ICH + Muse group) in 500 μL PBS were transplanted to ICH rats by tail vein injection within 1 h after ICH surgery. An equal volume of PBS was injected to Sham or ICH + PBS group.

Mice were divided into four groups by lottery method: Sham ($n = 6$), ALI + PBS ($n = 6$), ALI + MenSCs ($n = 6$), and ALI + Muse ($n = 6$). For ALI mouse treatment, 2×10^5 MenSCs (ALI + MenSCs group) or Muse cells (ALI + Muse group) in 200 μL PBS were transplanted to ALI mouse by tail vein injection after CCl_4 treatment for 24 h. An equal volume of PBS was injected to Sham or ALI + PBS group.

2.15. Behavior test

After cell transplantation for 3 days in ICH rats, behavior tests ($n = 6$ per group) including rotarod test and modified neurologic severity score (mNSS) were performed. For rotarod test, rats were placed on an accelerating (0–20 rpm) rotarod apparatus (RWD, Shenzhen, China) and were tested in consecutive three trials for a maximum of 300 s with an interval of 20 min. The latency to fall from the rod on each trial was recorded.

The neurological abnormality of rats was assessed by mNSS [22]. Neurological function was graded on a scale of 0–18 (normal score, 0; maximal deficit score, 18).

2.16. Live animal imaging

At day 1, 3, 5, 7 after cell transplantation, animals were anesthetized with isoflurane and fluorescent images were captured by *in vivo* imaging system (Tanon ABL X6, China). The living image software that comes with the system was used for analysis of the images post-acquisition.

2.17. Histopathological examination

The mice or rats were euthanized three days following cell transplantation. The largest right lobe of each liver was promptly excised and immersed in 4% paraformaldehyde for a duration of 24 hrs. The brains of each rat were extracted subsequent to heart perfusion and were fixed in 4% paraformaldehyde for a period of 48 hrs. Liver or brain samples underwent a gradual dehydration process using varying concentrations of ethanol and xylene, followed by embedding in paraffin. The liver samples were sectioned using the largest face, while the brain samples were sectioned coronally. Each section had a thickness of 4 μm. Following sectioning, the samples were stained with hematoxylin and eosin (H&E) and subsequently examined for any histopathological alterations using a light microscope (Olympus, Japan). To evaluate the liver histopathology, the percentage of cytoplasmic vacuolated hepatocytes in relation to the total number of hepatocytes was calculated by observing 5 high-power fields at a magnification of ×400. Similarly, for brain histopathological evaluation, the number of infiltrated inflammation cells was determined by observing 5 fields at ×200 magnification.

2.18. Cell migration detection in vivo

Rats ($n = 6$ per group) were anesthetized with 3% pentobarbital sodium (0.15 ml/100 g) and mice (n = 6 per group) were anesthetized with 0.3% pentobarbital sodium (0.15 ml/10g). Animals were transcardially perfused with 0.9% saline followed by 4% paraformaldehyde. The liver tissue of mouse and brain tissue of rat were collected and fixed in 4% paraformaldehyde for 24 h, and then dehydrated with 18% and 30% sucrose gradients. After embedding with OCT, the continuous frozen sections were made with a thickness of 20 μm. For each group, 20 sections were randomly chosen and incubated with primary antibody CD105 (10862-1-AP, Proteintech) overnight at 4 °C, followed by incubation with Goat anti-Rabbit IgG, Alexa Fluor 488 (Thermo Fisher A11034) for 2 h at room temperature. Dapi was used to stain the cell nucleus. For each section, 5 random fields were captured with an inverted fluorescence microscope (Leica, DMI3000B, Germany) at ×200 magnification. The number of DiL and CD105 double positive cells were counted manually.

2.19. GPT and GOT detection

To evaluate the extent of liver injury after cell transplantation for 3 days, the amount of glutamic pyruvic transaminase (GPT) and glutamic oxaloacetic transaminase (GOT) in the serum of mice ($n = 6$ per group) was detected by relevant kits (C009-1-1, C010-1-1, Nanjing Jiancheng) according to manufacturer's instruction.

2.20. Tumorigenicity of Muse cells

After anaesthetized using 1.5% isoflurane, each testis of a NOD/SCID mouse was injected with 1×10^5 MECs suspended in 1 μL saline or saline alone using glass microtubes. The mice were sacrificed to analyze tumorigenesis 6 months after the injection (three mice per group).

2.21. Quantitative real-time PCR

After incubated with trypsin for 0 h and 8 hrs, respectively, the alive MenSCs were collected and total RNA was extracted using TRIzol reagent (DP424, Tiangen) according to the manufacturer's instruction. After reverse transcription into cDNA, the expression of Nanog, Oct4, and Sox2 was detected by q-PCR using Roche LightCycler® 960 system under the following condition: 95 °C for 2 min, 40 cycles of denaturing at 95 °C for 5 s and combined annealing/extension at 60 °C for 10 s, melting curve analysis and holding at 4 °C. The critical threshold (ΔCT) value of interest genes was normalized to the glyceraldehyde 3-phosphate dehydrogenase (GAPDH). The results were calculated using $2^{-\Delta\Delta CT}$ method. The primers of q-PCR are as follows: Nanog-F: TTTGTGGGCCTGAAGAAAACT, Nanog-R: AGGGCTGTCCTGAATAAGCAG. Oct4-F: GGGAGATTGATAACTGGTGTGTT, Oct4-R: GTGTATATCCCAGGGTGATCCTC. Sox2-F: TACAGCATGTCCTACTCGCAG, Sox2-R: GAGGAAGAGGTAACCACAGGG. There are three biological replicates for each group and three technical replicates for each experiment.

2.22. RNA-seq and analysis

MenSCs and MECs were collected for mRNA high-throughput sequencing (Personal Biotechnology Co., Ltd. Shanghai, China), three biological replicates for each group. The raw read counts were normalized to log2-counts per million with the functions calcNormFactors from the R package edgeR (v.3.40.2) and voom from the R package limma (v3.54.2). The differential expression genes (DEGs) between these two groups were analyzed using the "Limma" package in R software version 4.2.2. Genes with P value < 0.05 and $|\log_2 \text{FoldChange}| > 1$ were considered DEGs. The figures of volcano plot, heatmap, Gene ontology (GO) and Kyoto Encyclopedia of Genes and Genomes (KEGG) enrichment analysis were generated using the "ggplots", "pheatmap", and "clusterProfiler" packages in R software.

2.23. Statistical analysis

Graphs generation and statistical analysis were performed using Prism 8.0.2 software (GraphPad, San Diego, CA, USA). Data were expressed as means ± standard deviation (SD) ($n = 3$ for *in vitro* experiments, $n = 3$–6 for *in vivo* experiments). Data normality was detected by Shapiro–Wilk test. Homogeneity of variance was detected by Brown–Forsythe test. For data that fit a normal distribution and homogeneity of variance, one-way ANOVA followed by Tukey's post hoc multiple comparison was used for comparison among 3 groups. Student *t*-test was used for comparison between 2 groups. Values of $p < 0.05$ were considered statistically significant.

3. Results

3.1. Immunophenotyping of MenSCs and MECs

The immunophenotype of MenSCs was identified by flow cytometry. Fig. 1A showed that CD73-APC, CD90-FITC and CD105-PerCP were all positive in MenSCs, with more than 98% positive cells in each index (Fig. 1Ab-Ad). Meanwhile, CD11b, CD34, CD45 and HLA-DR were negative in MenSCs, with less than 2% positive cells in each index (Fig. 1Ae-Ah), which met the minimum standard of MSCs reported by the International Society for Cell Therapy. Additionally, 56.3% of MenSCs was positive for CD146 (Fig. 1Ai) and 36.1% of MenSCs was positive for PDGF-β (Fig. 1Aj).

After treated by trypsin for 8 h, the expression of CD90, CD105, CD146 and PDGF-β greatly decreased (Fig. 1Bc, Bd, Bi, Bj), while the expression of SSEA3 increased from 2.24% to 7.59% (Fig. 1D). The expression of CD73, CD11b, CD34, CD45 and HLA-DR has no significant difference between MenSCs and MECs. After the cell suspension of MECs were transferred to adherent culture for 24 h, the expression of CD105 recovered to 57.95% (Fig. 1Cb). Meanwhile, CD90, CD146, and PDGF-β also recovered on a small scale (Fig. 1Ca, Cc, Cd).

3.2. LTT decreased the cell viability of MenSCs as a time-dependent manner

Cell survival rate of MenSCs was analyzed after incubation with 0.25% trypsin for 8 h, 16 h, and 24 h. As shown in Supplementary Table S1, the cell survival rate at each time point was 19.2% ± 3.5% ($n = 6$), 3.2% ± 1.7% ($n = 6$), and 0.8% ± 0.1% ($n = 3$), respectively. 8 h was chosen for the Muse cells isolation time point in this study.

3.3. Identification of Muse cells and M-clusters by double immunofluorescence staining

The growth characteristics of the suspension and adherent culture of Muse cells are shown in Fig. 2. P3–P6 MenSCs were treated by 0.25% trypsin for 8 h, and then transferred to suspension culture condition (Fig. 2A and B). Within 1–3 days, Muse cells were able to survive and began to proliferate to form small M-clusters, which are similar to human ES-like clusters (Fig. 2C). After suspension culture for 7–10 days, the diameter of M-clusters was 50–150 μm and were termed mature M-clusters (Fig. 1D). When mature M-clusters were transferred to gelatin coated cell culture dishes, Muse cells gradually migrated out of the M-cluster and continued proliferating (Fig. 1E and F). After repeated subculture, Muse cells eventually occupied a small proportion, which is similar to MenSCs.

SSEA3 and CD105 were commonly considered as makers of Muse cells. Mature M-clusters in suspension culture were collected, and SSEA3 and CD105 double immunofluorescence staining was performed. As shown in Fig. 2G, M-clusters expressed both CD105 and SSEA3. Besides, mature M-clusters were collected and seeded in 48-well plate to allow attaching and adherent culture. When all cells in the M-cluster migrated out, SSEA3 and CD105 double immunofluorescence staining was performed. As shown in Fig. 2H, the expression of CD105 and SSEA3 was positive.

3.4. Detection pluripotent markers and safety of Muse cells

As shown in Fig. 3, the M-cluster was positive for Nanog (Fig. 3A1-A3), Oct4 (Fig. 3B1-B3) and Sox2 (Fig. 3C1-C3), which were core nuclear transcription factors responsible for maintaining cell pluripotency. Besides, the level of ALP expression in cells is also considered as an indicator of cellular pluripotency. ALP staining was performed on MenSCs, M-clusters and iPSCs. The response of MenSCs to ALP staining was weak (Fig. 3D), which was similar to the staining result of cells migrated out of the M-cluster (Fig. 3E). The center of the M-cluster was reddish purple (Fig. 3E), indicating that ALP was strongly expressed in the M-cluster. Meanwhile, iPSCs was used as a positive control, which showed a strongly ALP positive result of dark purple color (Fig. 3F). Although Muse cells are pluripotent, they showed non-tumorigenicity after injecting to the testis of NOD/SCID mice for 6 months (Fig. 3G). Furthermore, we compared the mRNA expression level of *Nanog*, *Oct4*, and *Sox2* between naïve MenSCs and MECs. Results showed LTT treating could significantly increase the expression of *Nanog* (Fig. 3H and 1.446 ± 0.2277, $*p < 0.05$), *Oct4* (Fig. 3I and 2.205 ± 1.1044, $***p < 0.001$), and *Sox2* (Fig. 3J and 6.665 ± 0.5452, $***p < 0.001$).

3.5. Multilineage differentiation in vitro

In order to identify the multilineage differentiation ability of Muse cells *in vitro*, they were exposed to adipocytes, osteocytes, chondrocytes, and neurons differentiation reagents, respectively. Fig. 4A was adipogenesis induction, and oil red O staining showed lipid droplets in the cytoplasm after 14 days of induction. The differentiation into osteoblasts was demonstrated by Alizarin Red S staining of the red color mineralization nodes after 21 days of induction (Fig. 4B). The differentiation into chondrocytes was revealed by the formation of cartilage spheroid stained by Alcian blue after 14 days of induction (Fig. 4C). Fig. 4D and E showed that Muse cells could generate DCX (Fig. 4D) and Nestin (Fig. 4E) positive neural precursor cells (NPCs) sphere within 5–7 days. After exposed to the second stage induction medium for 10–14 days, immunofluorescence staining indicated that Muse cells could be induced to MAP-2 (Fig. 4F) and Tju-1 (Fig. 4G) positive mature neurons, S100β (Fig. 4H) positive astrocytes and GAP43 (Fig. 4I) positive Schwann cells.

3.6. Comparison the migration ability of Muse cells and MenSCs in vitro

The serum of ALI mouse, ICH rat, and healthy animals was indirectly co-cultured with MenSCs or Muse cells respectively to compare their migration ability towards inflammatory environment *in vitro*. Fig. 5A illustrated the schematic diagram of the *in vitro* migration experiment. Compared with control group, the number of MenSCs and Muse cells migrating towards the lower chamber significantly increased (Fig. 5B–E, $^{\#}p < 0.05$, $^{\#\#}p < 0.01$, $^{\#\#\#}p < 0.001$). Moreover, Muse cells had stronger migration ability than MenSCs in both ALI and ICH serum co-culture system ($*p < 0.05$, $***p < 0.001$). These results indicated superior inflammatory response potential of Muse cells in comparison to MenSCs.

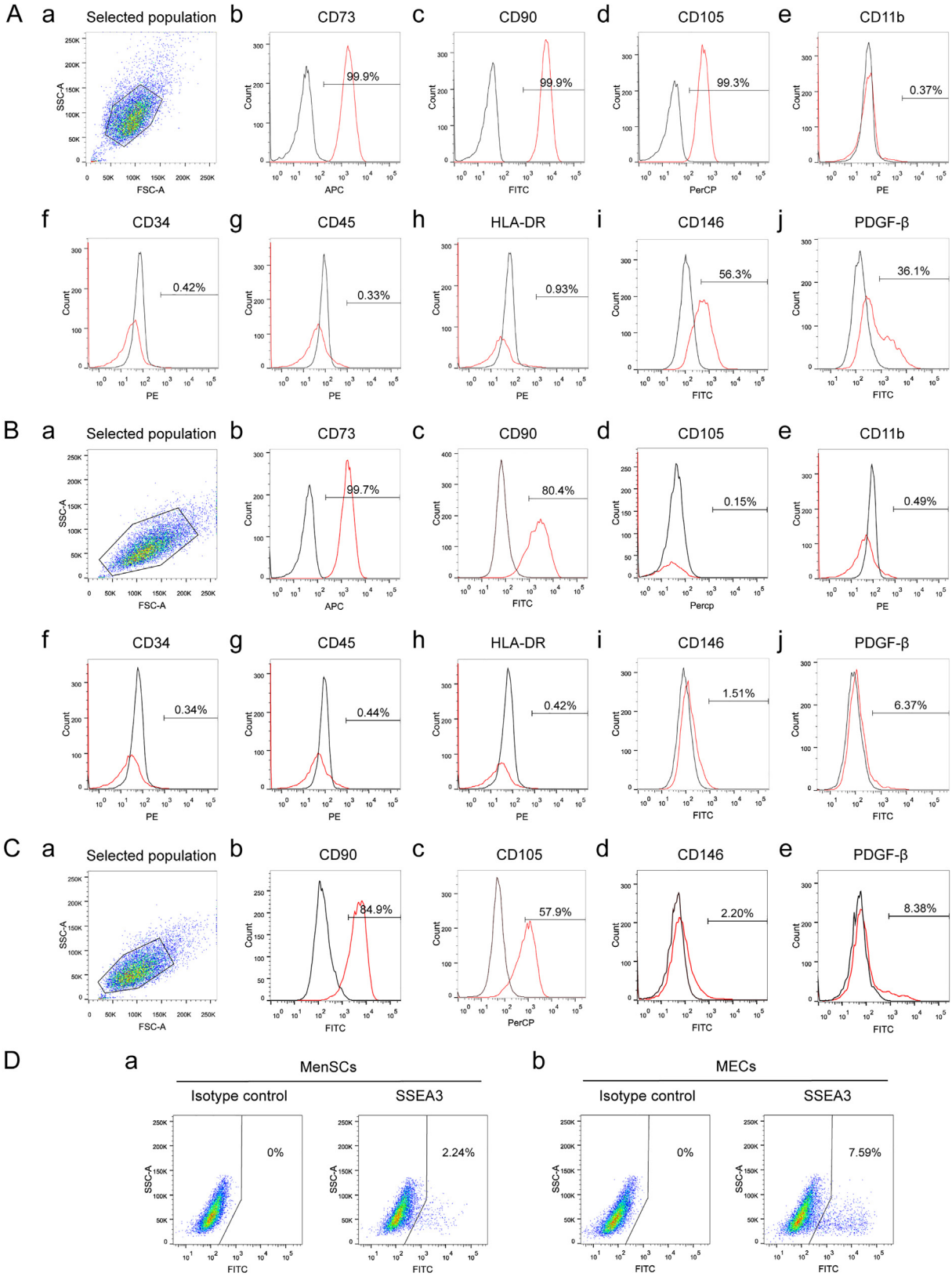

Fig. 1. Characterization of MenSCs and MECs by immunophenotyping. (A) The surface markers of MenSCs were detected by flow cytometry. (B) MenSCs was subjected to LTT for 8 h, and then surface markers were detected by flow cytometry. (C) After LTT incubation for 8 h, MECs were cultured in adherent condition for 24 h and then surface markers were detected by flow cytometry. (D) The expression levels of SSEA3 in MenSCs and MECs were detected by flow cytometry. Black lines stand for isotype controls and red lines represent for markers expression. Three independent experiments were performed.

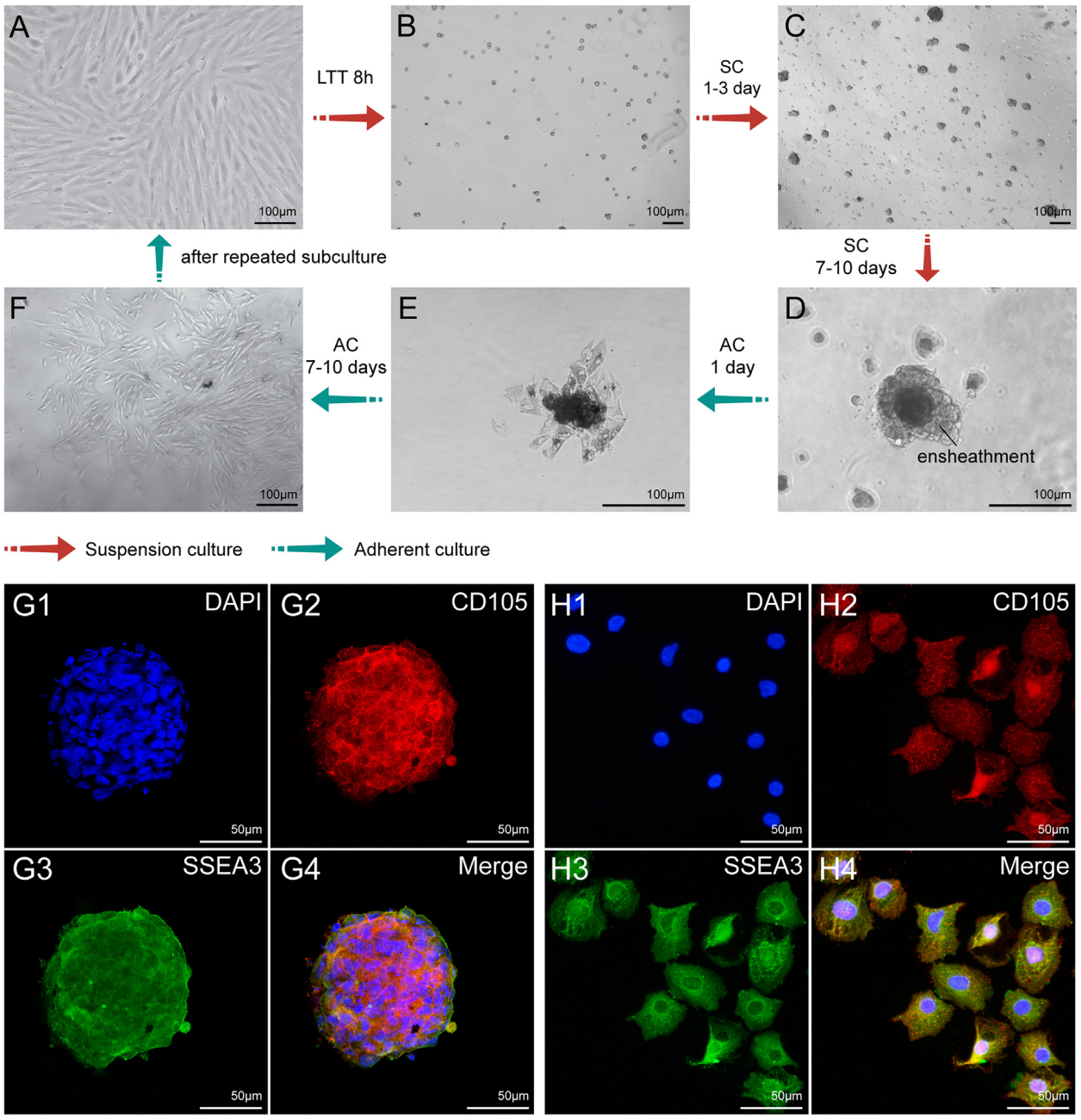

Fig. 2. Growth process of Muse cell and its identification by immunofluorescence. (A) The morphology of MenSCs in adherent culture condition. (B) LTT-treated MenSCs in suspension culture condition. (C) Muse cells formed 10–30 μm M-clusters after suspension culture for 1–3 days. (D) Muse cells formed 100–150 μm M-clusters after suspension culture for 7–10 days. Black line indicated an ensheathment formed by non-Muse cells. (E) The mature M-cluster was transferred to adherent culture. Inner Muse cells migrated out of the cluster. (F) All Muse cells migrated out of the cluster. After repeated subculture, the proportion of non-Muse cells accounts for a proportion of cells consistent with that found in MenSCs. (G1-G4) M-clusters were subjected to double immunofluorescence staining of CD105 (red) and SSEA3 (green). (H1–H4) Muse cells were subjected to double immunofluorescence staining of CD105 (red) and SSEA3 (green). Nuclei were counterstained with DAPI (blue). Three independent experiments were performed. Scale bar: 100 μm in A–F, 50 μm in G1–G4 and H1–H4.

3.7. The therapeutic effect of Muse cells on ALI disease model

After transplanted to ALI mice model by tail vein injection, both MenSCs and Muse cells could migrate to the injury sites (Fig. 6A–C). Moreover, the number of Muse cells migrating to the damaged site was significantly more than MenSCs (Fig. 6H, $^{*}p < 0.05$), which was indicated by the double positive for DiL and CD105 (arrows in B4 and C4).

Compared to the control group, there was evident disruption in the architecture of hepatic lobules and hepatic cords in the ALI + PBS group (Fig. 6D and E). The hepatocytes located in each lobule displayed noticeable swelling, along with irregular vacuolation in the cytoplasm and nuclei seemingly suspended within the cleared central region (Fig. 6E). Treatment with MenSCs and Muse cells exhibited a significant reduction in the pathological damage inflicted upon the liver. The severity of disorder in liver lobules and hepatic cords was mild, and the quantity of vacuoles was diminished (Fig. 6F, G, I). Based on the statistical analysis result, the proportion of cytoplasmic vacuolated hepatocytes relative to the total hepatocyte count was lower in the ALI + Muse group compared to the ALI + MenSCs group (Fig. 6I, $^{\&\&}p < 0.01$).

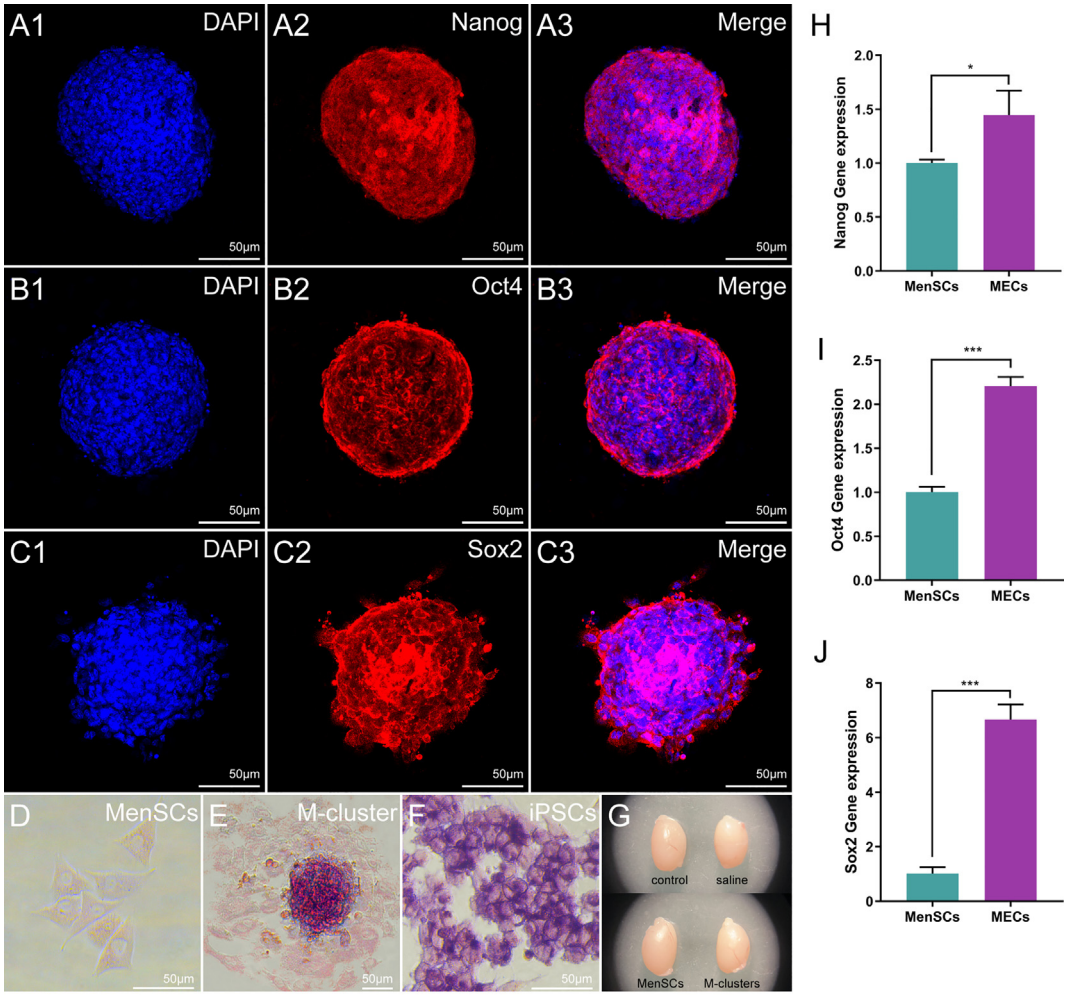

Fig. 3. Pluripotency and biological safety of Muse cells. Immunofluorescence showed the expression of pluripotency markers Nanog (A1-A3), Oct4 (B1–B3) and Sox2 (C1–C3) in M-clusters. (D–F) ALP staining on MenSCs, M-cluster, and iPSCs. (G) Uninjected testes (control), testes injected with saline, MenSCs, and M-clusters for 6 months. (H–J) The expression levels of Nanog, Oct4, and Sox2 were detected by q-PCR. All experimental data are expressed as the mean ± SD of three independent experiments (n = 3). $*p < 0.05$, $**p < 0.01$, $***p < 0.001$. Scale bar: 50 μm in A-F.

To detect liver function, the content of glutamic oxaloacetic transaminase (GOT) and glutamic pyruvic transaminase (GPT) in the serum of different group mice was analyzed. Results demonstrated that both MenSCs and Muse cells could significantly decrease the amount of GOT in the serum of ALI mice (Fig. 6J $**p < 0.01$, $^{\#\#\#}p < 0.001$). However, only the administration of Muse cells significantly decreased the amount of GPT (Fig. 6K, $^{\#}p < 0.05$). This observation implies that Muse cells exhibit a more effective therapeutic effect than MenSCs.

We also investigated the survival time of MenSCs and Muse cells in ALI model using live animal imaging (Supplementary Fig. S1A). In the ALI + PBS group, the DiL solution primarily accumulates in lung tissue through the process of blood circulation. Conversely, in both ALI + MenSCs and ALI + Muse groups, the DiL-labelled MenSCs and Muse cells exhibit the ability to migrate to liver tissue. However, by day 7 following cell transplantation, the presence of DiL in liver tissue becomes undetectable, suggesting the disappearance of MenSCs and Muse cells. Quantitative analysis reveals that Muse cells demonstrate a greater propensity for migration to damaged liver tissue compared to MenSCs at 1 d and 3 d (Fig. S1C).

3.8. The therapeutic effect of Muse cells on ICH disease model

Because of the damaged blood–brain barrier (BBB) of ICH rats, transplanted cells could reach brain by intravenous injection. Fig. 7A–C and H demonstrated that there were more Muse cells surviving in the hematoma area compared with MenSCs ($**p < 0.01$).

According to the H&E result, in the ICH + PBS group, a large number of inflammatory cells were observed. Both MenSCs and Muse cells transplantation significantly reduced inflammatory cell infiltration (Fig. 7D-G, I). Furthermore, less inflammatory cells infiltration was observed in the ICH + Muse group compared with the ICH + MenSCs group (Fig. 7I, $^{\&}p < 0.05$).

To evaluate the therapeutic effect of transplanted cells on the motor and neurological function of ICH rats, rotarod and mNSS tests were performed. Rotarod test results (Fig. 7J) showed that Muse cells significantly improved the motor performance of ICH rats after transplantation for 2 days ($^{\#}p < 0.05$ *vs* ICH + PBS group), while there was no significant difference between ICH + MenSCs group and ICH + PBS group ($^{ns}p > 0.05$). Although both MenSCs and Muse cells

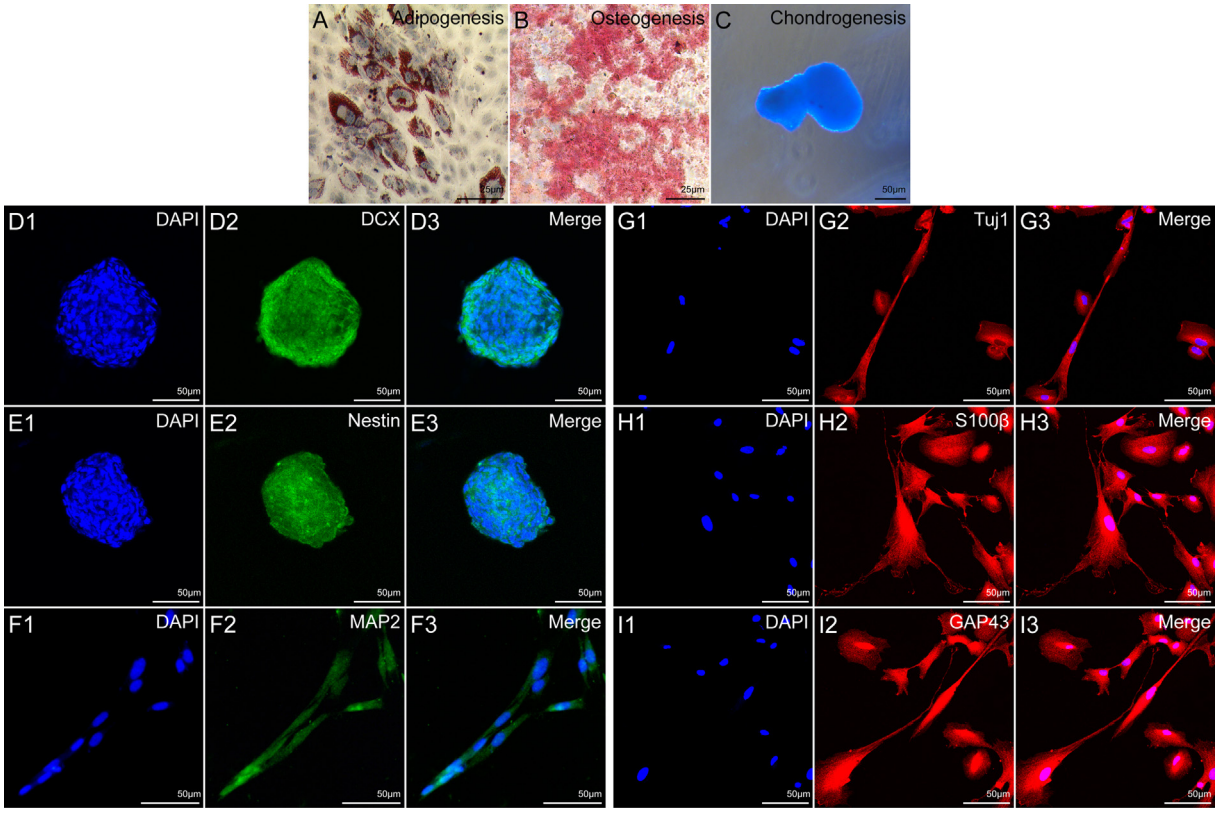

Fig. 4. Multilineage differentiation of Muse cells *in vitro*. (A–C) Muse underwent adipogenesis, osteogenesis, and chondrogenesis. Cell nucleus was stained by hematoxylin in A. (D–E) Neurosphere expressed DCX (D1-D3) and nestin (E1-E3). (F–I) After the second step induction, cells expressed MAP2 (F1–F3), Tju1 (G1-G3), S100β (H1–H3), and GAP43 (I1–I3). Three independent experiments were done for each staining (n = 3). Scale bar: 25 μm in A and B, 50 μm in C–I.

could ameliorate the motor ability of ICH rats at day 3 ($^{***}p < 0.001$, $^{\#\#\#}p < 0.001$ *vs* ICH + PBS group), Muse cells increased the time of latency to fall much more than MenSCs ($^{\&}p < 0.05$ *vs* ICH + MenSCs group). mNSS results (Fig. 7K) illustrated that Muse cells improved the neurological function of ICH rats at day 2 and day 3 ($^{\#\#}p < 0.01$ *vs* ICH + PBS group). In contrast, there was no significant difference between ICH + MenSCs group and ICH + PBS group at all indicated time points ($^{ns}p > 0.05$). Besides, rats of ICH + Muse group had better restoration of neurological function than that of ICH + MenSCs group at day 3 ($^{\&}p < 0.05$).

We also investigated the survival time of MenSCs and Muse cells in ICH model using live animal imaging (Supplementary Fig. S1B). In the ICH rat model, the presence of DiL-labelled Muse cells was observed one day after transplantation and ceased to exist by day 7. In contrast, MenSCs primarily migrated to the brain region by day 3 and were almost no longer detectable by day 7. Quantitative analysis revealed that Muse cells demonstrate a greater propensity for migration to brain tissue compared to MenSCs at day 1 (Fig. S1 D, $^{**}p < 0.01$), and the difference became no statistical difference since day 3 (Fig. S1 D, $^{ns}p > 0.05$).

3.9. Bioinformatic analysis

mRNA high-throughput sequencing was performed to detect the differential mRNA expression profiling of MenSCs and MECs. Volcano plot displayed 754 up-regulated genes and 568 down-regulated genes in MECs (Fig. 8A). The top 20 downregulated genes and top 20 upregulated genes were presented in a heatmap (Fig. 8B). The 1322 differential genes were subjected to Gene ontology (GO) and Kyoto Encyclopedia of Genes and Genomes (KEGG) enrichment analysis using the "clusterProfiler" package in R software. GO analysis enriched biological processes such as response to extracellular stimulus, regulation of neurogenesis, intrinsic apoptotic signaling pathway, mesenchymal cell differentiation, etc (Fig. 8C). Meanwhile, 11 molecular function GO categories were enriched within the data set and included the terms DNA-binding transcription activator activity, GTPase activity, protein heterodimerization activity, 14-3-3 protein binding, etc. KEGG analysis showed that differential genes were involved in MAPK signaling pathway, gastric/breast cancer, signaling pathways regulating pluripotency of stem cells, TNF signaling pathway, NF-kappa B signaling pathway, FoxO signaling pathway, apoptosis, etc (Fig. 8D).

It was reported that S1P–S1PR2 axis had a correlation with the homing of Muse cells to damaged tissue. Consequently, we conducted a specific analysis on the fold change in expression of S1PR1, S1PR2, S1PR3, and S1PR5 in MenSCs and MECs. The results revealed a significant increase in the expression of S1PR2 in MECs compared to MenSCs ($^{*}p < 0.05$, Fig. 8F), while the expression of S1PR3 significantly decreased ($^{*}p < 0.05$, Fig. 8G). No statistically significant difference was observed in the expression of S1PR1 and S1PR5 ($^{ns}p > 0.05$, Fig. 8E and H). Several reports have suggested that the presence of 14-3-3 protein may contribute to the stress tolerance observed in Muse cells. The expression levels of eight genes involved in the binding of 14-3-3 protein (GO:0071889, ontology: Molecular Function) were documented in Fig. 8I-P. In comparison to MenSCs, the expression levels of DAB2IP, DDIT4, HLA-F, IRS2, SIK1, TBC1D22B, and ZFP36L1 were found to be significantly elevated in MECs ($^{*}p < 0.05$, $^{**}p < 0.01$, $^{***}p < 0.001$). Conversely, the expression level of SYNPO2 exhibited a significant decrease ($^{**}p < 0.01$).

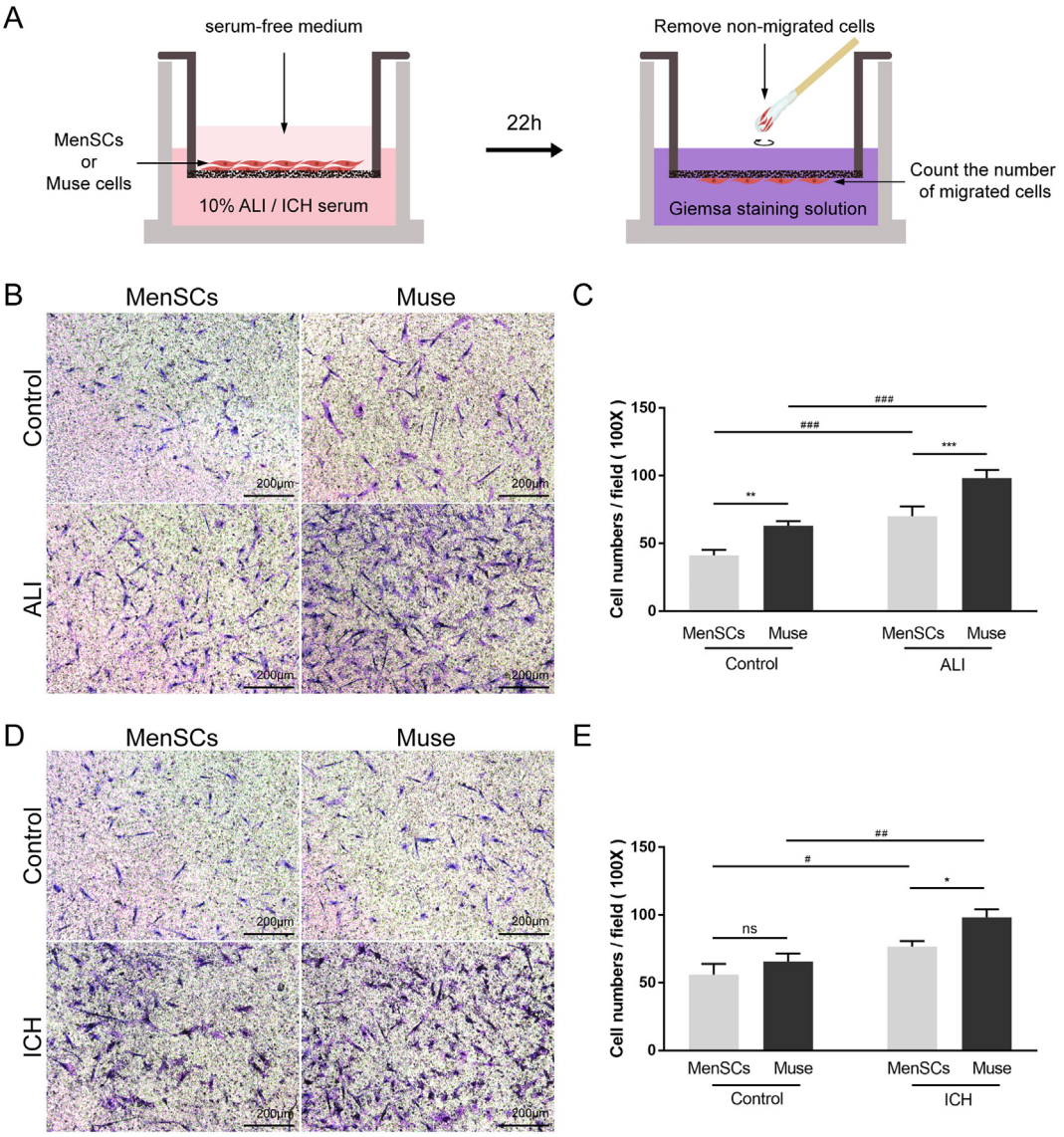

Fig. 5. *In vitro* migration ability assay of MenSCs and Muse cells. (A) Schematic diagram of the *in vitro* migration experiment. (B) Giemsa staining showed the migrated MenSCs or Muse cells towards the serum of control and ALI mouse. (C and E) The number of cells passing through the semipermeable membrane was counted and statistically analyzed. (D) Giemsa staining showed the migrated MenSCs or Muse cells towards the serum of control and ICH rat. All experimental data are expressed as the mean ± SD of three independent experiments (n = 3). $^{ns}p>0.05$, $^{*}p < 0.05$, $^{**}p < 0.01$, $^{***}p < 0.001$, $^{\#}p < 0.05$, $^{\#\#}p < 0.01$, and $^{\#\#\#}p < 0.001$. Scale bar: 200 μm in B and D.

4. Discussion

According to the report by Kuroda [8], the cell survival rate of BM-MSCs treated with trypsin for 8 h was found to be 10%, which was higher than the survival rate of 3% observed after 16 h of treatment. Conversely, the cell survival rate of human fibroblasts treated with trypsin for 8 h was lower at 1%, while it increased to 5% after 16 h of treatment. Furthermore, when exposed to long-term trypsinization (LTT) for 8 h, the proportion of Muse cells in both BM-MSCs and human fibroblasts increased from 0.7%–7% to 1.9%–8.3%, respectively. In our study, the survival rate of MenSCs after 8 h of LTT treatment was 19.2% ± 3.5%, whereas only 3.2% ± 1.7% of MenSCs survived after 16 h of LTT treatment. Besides, the expression of SSEA3 increased from 2.24% to 7.59% after exposed to LTT for 8 h. These aforementioned collective findings suggest that various cell types exhibit varying degrees of tolerance towards trypsin.

Fluorescent-activated cell sorting (FACS) [9,23,24], magnetic-activated cell sorting (MACS) [25–27], and LTT [28–31] are three frequently employed techniques for obtaining Muse cells. Uchida et al. highlighted that Muse cells isolated through MACS exhibited superior cell viability and collection efficiency in comparison to FACS [32]. However, the purity of Muse cells sorted by magnetic beads was found to be lower than that achieved through flow cytometry. The absence of SSEA3 application renders LTT the most cost-effective method when compared to the other two techniques, albeit with the least satisfactory purity of Muse cells [2,15]. Kuroda proposed that LTT is not indispensable for isolating Muse cells, but rather serves as a method to enhance the enrichment of Muse cells [8]. Hence, certain researchers classify the cells obtained through LTT as the Muse-enriched cell (MEC) population. In addition to LTT, Heneidi et al. successfully obtained a highly purified population of Muse cells from adipose tissue through long-term exposure to the proteolytic enzyme collagenase, serum deprivation, the implementation of low temperatures and hypoxia [12]. Besides, Wang et al. exposed human abdominal subcutaneous fat to collagenase and nutrient deficiency medium for 16 h and obtained a cell

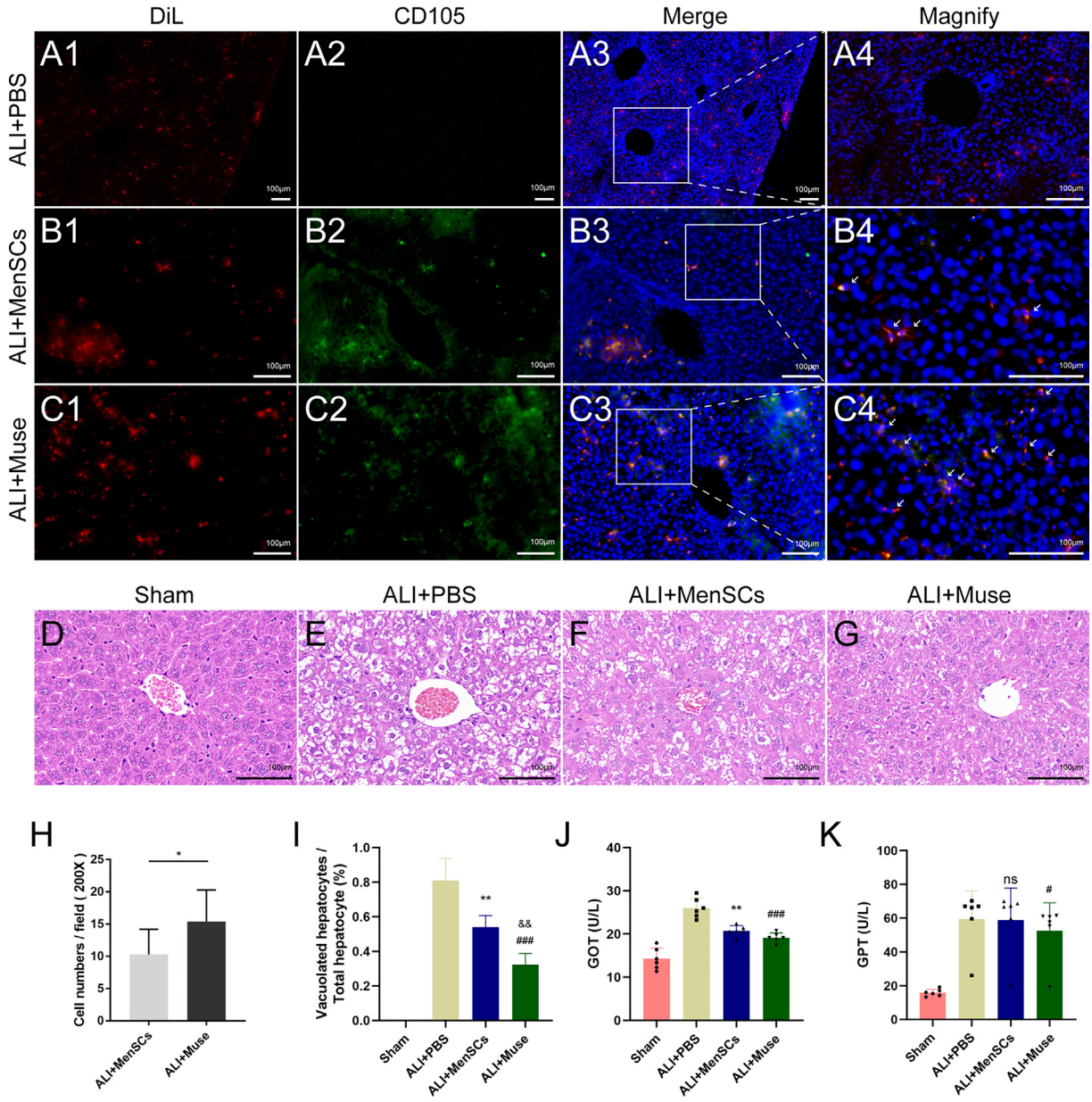

Fig. 6. The therapeutic effect of Muse cells on ALI disease model. DiL-labelled MenSCs/Muse cells/PBS were transplanted into ALI mice model by tail vein injection. (A–C) Immunofluorescence showed the migrated CD105 positive MenSCs and Muse cells towards injury liver (6 mice per group). (D–G) Liver sections were subjected to hematoxylin and eosin staining to detect histopathological changes (×400 magnification). (H) Statistical analysis of the number of migrated cells in ALI disease model. *$p < 0.05$, ALI + MenSCs *vs* ALI + Muse. (I) Statistical analysis of the proportion of cytoplasmic vacuolated hepatocytes relative to the total hepatocyte count in different groups. **$p < 0.01$, ALI + MenSCs *vs* ALI + PBS; $^{\#\#\#}p < 0.001$, ALI + Muse *vs* ALI + PBS; $^{\&\&}p < 0.01$, ALI + Muse *vs* ALI + MenSCs. (J and K) The content of glutamic oxaloacetic transaminase (GOT) and glutamic pyruvic transaminase (GPT) in the serum of different groups mice (6 mice per group). **$p < 0.01$, $^{ns}p>0.05$, ALI + MenSCs *vs* ALI + PBS; $^{\#}p < 0.05$, $^{\#\#\#}p < 0.001$, ALI + Muse *vs* ALI + PBS. Values are expressed as the means ± SD in each group. Scale bars: 100 μm in A-G.

population containing 70% Muse cells [33]. Furthermore, Kuroda et al. highlighted that the utilization of different SSEA3 antibodies and various culture procedures for parent cells, such as thawing, growth, passaging, freezing, and serum selection, could significantly impact the yield of Muse cells [8,9]. The potential influence of factors such as the variability of sources, donor age, and passage of parent cells on gene expression profiles and therapeutic efficacy remains unknown.

Stage specific embryonic antigen (SSEA) is an oligosaccharide chain that is present in the forms of glycoprotein and glycolipid, particularly in the glycosylsphingolipid [34]. SSEA is widely expressed in both embryonic and adult mammalian tissues, including SSEA1, SSEA3, and SSEA4, and plays a crucial role in embryonic development and differentiation [34]. SSEA3 is commonly used as a marker for the isolation and identification of Muse cells. Notably, Pan et al. [35] successfully isolated a population of SSEA4-positive cells from bovine embryonic skin fibroblasts using MACS, which exhibited similar characteristics to SSEA3-positive Muse cells, such as expressing pluripotency-related markers, differentiating into cells comprising all three germ layers, positive for alkaline phosphatase, suspension growth, etc. Further exploration is required to understand the distinctions between SSEA3 and SSEA4 positive cell populations. The role of SSEA3 or SSEA4 in stem cell biology, aside from its function as a marker of Muse cells, has been inadequately investigated. Aprile et al. demonstrated that SSEA3, in conjunction with FGF2, influences the

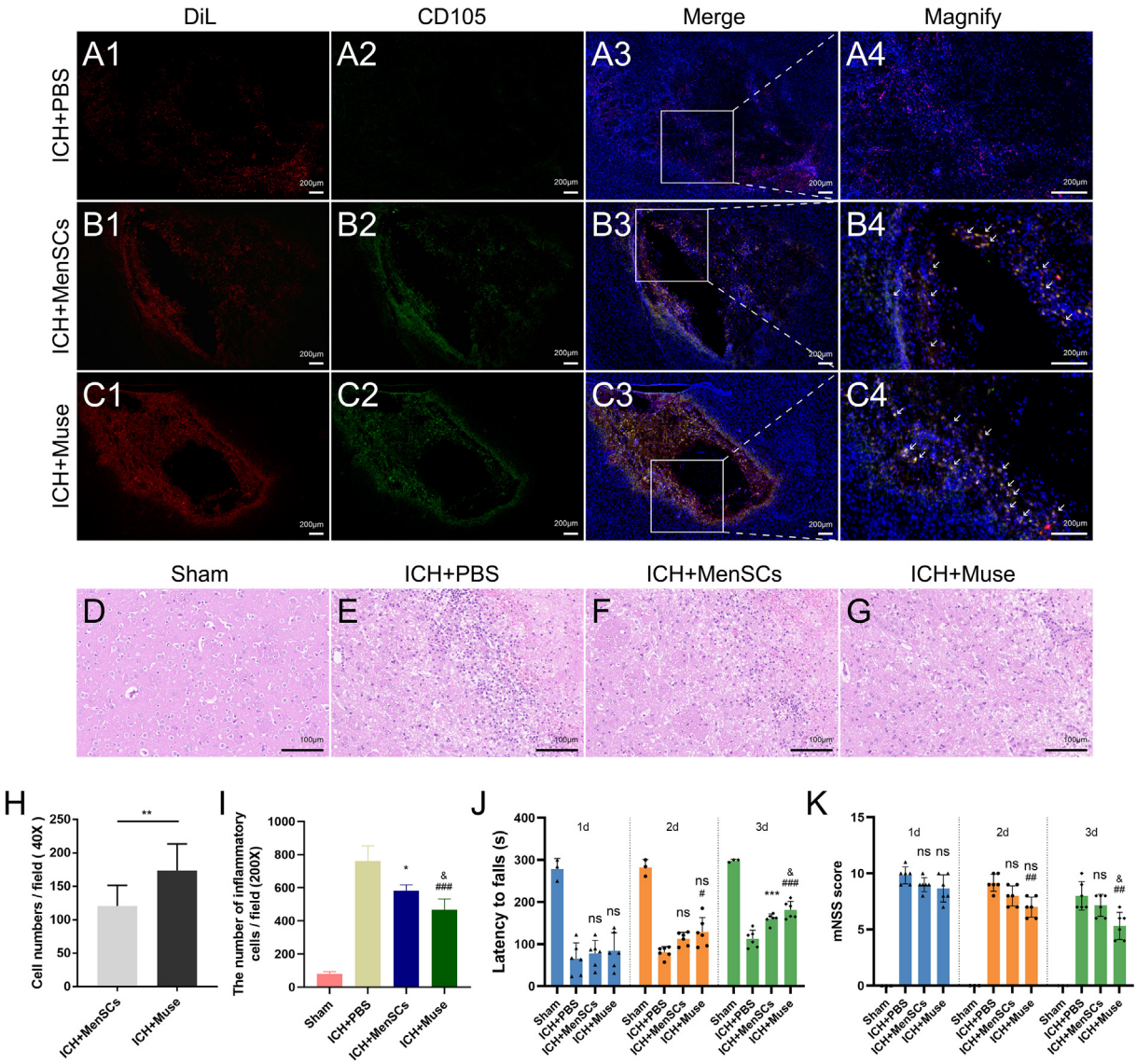

Fig. 7. The therapeutic effect of Muse cells on ICH disease model. DiL-labelled MenSCs/Muse cells/PBS were transplanted into ICH rat model by tail vein injection. (A–C) Immunofluorescence showed the migrated CD105 positive MenSCs and Muse cells towards injury liver (6 mice per group). (D–G) Brain sections were subjected to hematoxylin and eosin staining to detect histopathological changes (×200 magnification). (H) Statistical analysis of the number of migrated cells in ICH disease model. $^{**}p < 0.01$, ICH + MenSCs *vs* ICH + Muse. (I) Statistical analysis of infiltrated inflammatory cells. $^{*}p < 0.05$, ICH + MenSCs *vs* ICH + PBS; $^{\#\#\#}p < 0.001$, ICH + Muse *vs* ICH + PBS; $^{\&}p < 0.05$, ICH + Muse *vs* ICH + MenSCs. (J) Rostar rod behavior test (6 rats per group). $^{***}p < 0.001$, $^{ns}p > 0.05$, ICH + MenSCs *vs* ICH + PBS; $^{ns}p > 0.05$, $^{\#}p < 0.05$, $^{\#\#\#}p < 0.001$, ICH + Muse *vs* ICH + PBS; $^{\&}p < 0.05$, ICH + Muse *vs* ICH + MenSCs. (K) mNSS test. $^{ns}p > 0.05$, ICH + MenSCs *vs* ICH + PBS; $^{ns}p > 0.05$, $^{\#\#}p < 0.01$, ICH + Muse *vs* ICH + PBS; $^{\&}p < 0.05$, ICH + Muse *vs* ICH + MenSCs. Values are expressed as the means ± SD in each group. Scale bars: 200 μm in A–C and 100 μm in D–G.

self-renewal and clonogenic potential of Muse cells. Inhibition of SSEA3 significantly diminished the multilineage potential of Muse cells, resulting in the generation of nullipotent clones [27].

So far, Muse cells have been successfully isolated and identified from various sources such as human/rabbit BM-MSCs [24,27,28,36], human adipose-derived MSCs [12,13,25,26,33], human UC-MSCs [11], human dermal fibroblasts [8,23,29,37], and human synovial membrane. In comparison to other MSCs, MenSCs can be easily obtained noninvasively and collected periodically, rendering them a valuable resource for regenerative medicine. Consequently, we have developed a method for isolating Muse cells from MenSCs using the LTT method. We firstly observed a significant decrease in the expression of CD90, CD105, CD146, and PDGF-β after an 8-h treatment with trypsin (Fig. 1B). However, the expression of CD73 remained unaffected. Notably, the expression of CD105 decreased from 99.3% to 0.15%. Following a subsequent adherent culture for 24 h, the expression of the aforementioned cell surface markers increased (Fig. 1C). Specifically, the expression of CD105 increased from 0.15% to 57.9%. It is currently unknown whether MSCs or fibroblasts from other sources exhibit the same phenomenon.

Iseki et al. revealed that Muse cells derived from BM-MSCs exhibited enhanced migratory capacity towards the serum of an immunodeficient mouse model of ALI, as compared to non-Muse cells [5]. Our study yielded the similar findings utilizing 10% serum from a BALB/c model of ALI. Sphingosine 1-phosphate (S1P) is a pleiotropic and widely expressed bioactive molecule belonging to the sphingolipid family [38]. S1P receptors (S1PRs) are high affinity G protein-coupled cell surface receptors comprising five distinct subtypes known as S1PR1-S1PR5 [39]. S1PR1-2 and 3 exhibit a broad tissue distribution, whereas S1PR4 is primarily found in lymphoid tissues, and S1PR5 is expressed predominantly in the nervous system [39]. In a study conducted by Yamada, Muse cells were isolated from rabbit BM-MSCs using FACS. The findings revealed that the expression level of S1PR2 in Muse cells was

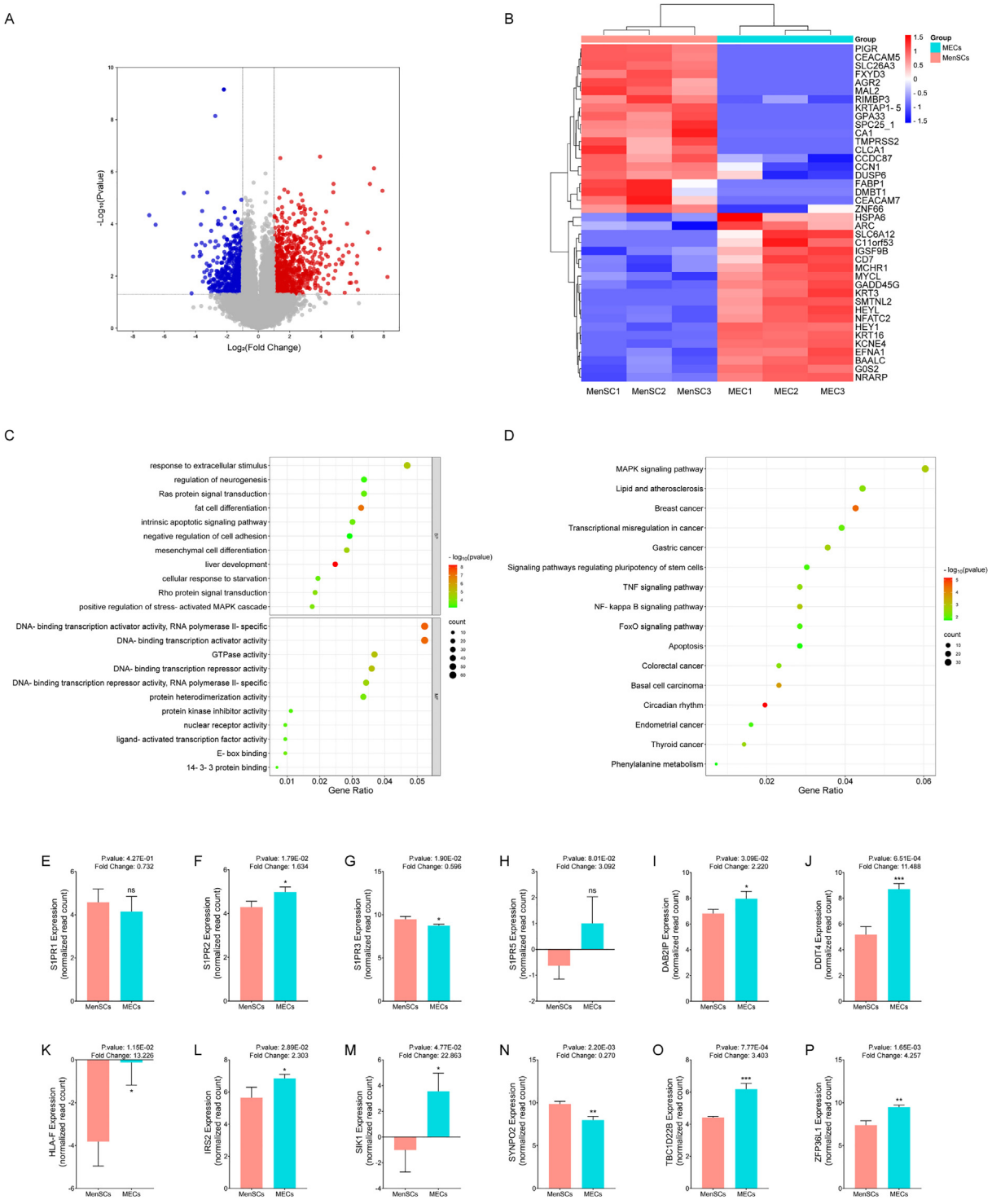

Fig. 8. Bioinformatic analysis. (A) Volcano plot displayed differential expression genes between MenSCs and MECs. (B) Heatmap demonstrated the top 20 downregulated genes and top 20 upregulated genes. (C) Gene ontology biological processes (GO-BP) and molecular functions (GO-MF). (D) Kyoto Encyclopedia of Genes and Genomes (KEGG) enrichment analysis. (E–H) Gene expression level of S1PR1, S1PR2, S1PR3 and S1PR5 in MenSCs and MECs. (I–P) Expression levels of 14-3-3 protein binding related genes. There are three samples per group, which were prepared by three independent experiments. $^{ns}p>0.05$, $*p < 0.05$, $**p < 0.01$, $***p < 0.001$ *vs* MenSCs.

significantly higher than that in non-Muse cells, while the expression levels of other S1PR subtypes were lower compared to non-Muse cells [36]. The utilization of a S1PR2-specific antagonist or S1PR2-siRNA resulted in a notable decrease in the migration of Muse cells both *in vitro* and *in vivo*, which indicated S1P–S1PR2 axis may play a central role in controlling preferential migration of Muse cells [36]. However, an analysis of single cell sequencing data showed that there was no significant disparity in the expression of all S1PR subtypes between Muse and non-Muse cells [40]. Besides, examination of microarray results from adipose tissue derived Muse cells and AD-MSCs revealed no significant difference in the expression of S1PR2 between these two groups. The expression of S1PR5 was found to be higher in Muse cells, whereas S1PR3 and S1PR4 exhibited lower expression levels in Muse cells [12]. Our RNA

sequence analysis revealed that the expression levels of S1PR2 and S1PR5 in MECs were significantly higher than those in MenSCs, while the expression levels of other S1PR subtypes were lower in MECs compared to MenSCs. These divergent findings may be attributed to the distinct origins and preparation methods of Muse cells. Further investigation is required to elucidate the biological role of other S1PR subtypes in regulating the migration of Muse cells.

The ability of Muse cells to withstand adverse conditions has garnered significant attention. Nicola et al. conducted a study revealing that Muse cells possess the capability to promptly and effectively identify DNA damage and initiate the DNA damage repair mechanism. Consequently, Muse cells exhibit greater resistance to genotoxic stress in comparison to MSCs and non-Muse cells [41]. Wang et al. [33] and Heneidi et al. [12] demonstrated a significant increase in the CCNA2 gene expression level in AD-MSCs derived Muse cells compared to AD-MSCs. Additionally, when subjected to H_2O_2 stress *in vitro*, Muse cells exhibited a notably higher survival rate than AD-MSCs. The upregulation of CCNA2 gene expression in AD-MSCs has been shown to enhance the survival rate of AD-MSCs under H_2O_2-induced stress, while also significantly reducing apoptosis and the expression of senescence-related gene [33]. Thus, Wang et al. hypothesized that the high expression of the CCNA2 gene may be associated with the increased stress tolerance of AD-MSCs derived Muse cells. However, our RNA sequence analysis revealed no changes in the expression levels of CCNA2 in MECs compared to MenSCs. This finding was further supported by the single cell sequence analysis of BM-MSCs, which showed no differences in CCNA2 expression between BM-MSCs derived Muse and non-Muse cells [40].

The 14-3-3 protein family is characterized by its high conservation and acidic nature. Its ability to interact with more than 200 functionally diverse proteins enables it to play crucial roles in various essential regulatory processes, including cell cycle control, mitogenic signal transduction, apoptosis, migration, and survival [42,43]. The growing body of evidence suggests that 14-3-3 serves as a significant convergence point for numerous protein kinases and phosphatases involved in the activation, maintenance, and release of the G1/S and G2/M cell cycle checkpoints [44]. Additionally, 14-3-3 proteins could functionally inactivate the critical pro-apoptotic effector BAD and BAX and assist damaged proteins in maintaining their physiologically relevant structure [44]. In our study, GO-MF revealed that the different genes between MECs and MenSCs involved in 14-3-3 protein binding process. It is plausible that 14-3-3 proteins may partly contribute to the stress tolerance exhibited by Muse cells.

5. Conclusion

This study developed a technique to isolate Muse cells from MenSCs and demonstrated that Muse cells exhibit enhanced homing ability and therapeutic efficacy in the treatment of acute liver injury and intracerebral hemorrhage diseases compared to MenSCs. Additionally, the findings from RNA-seq and GO-MF analysis suggest that 14-3-3 proteins may play a role in the stress tolerance observed in Muse cells. Moreover, this study offers insights into the mechanism underlying the disparity in migration ability between Muse and MenSCs cells, proposing that the upregulation of SIRP2 and SIPR5 may contribute to the superior migratory capacity of Muse cells.

Funding

This work was supported by grants from Henan Outstanding Youth Science Fund (202300410307), Key Scientific Research Project of Henan Province Colleges and Universities (24A180026), Xinxiang Medical University Doctor Support Foundation (XYBSKYZZ201902), and Graduate Research Innovation Support Program (YJSCX202209Z, YJSCX202206Z). The funding body played no role in the design of the study and collection, analysis, and interpretation of data and in writing the manuscript.

Author contributions

Conceptualization, H.L; Methodology, J.H.W., M.Z.L., Y.Q.L., T.Z., J.L.T., X.J.L., and K.J.L.; Validation, J.H.W. and M.Z.L.; Formal Analysis, J.H.W.; Investigation, H.L., J.H.W., M.Z.L., Y.Q.L., T.Z., and. J.L.T.; Resources, H.L. and J.T.L.; Writing-Original Draft, J.H.W.; Writing-Review & Editing, H.L. and J.T.L.; Supervision, J.T.L.; Funding Acquisition, J.T.L., H.L., and X.J.L.

Data availability

The transcriptome data in this study have been deposited in NCBI's Gene Expression Omnibus (GEO) with the accession number GSE247588.

Additional data and materials may be requested from the corresponding author on reasonable request.

Declaration of competing interest

The authors declare the following financial interests/personal relationships which may be considered as potential competing interests: Juntang Lin reports financial support was provided by Henan Outstanding Youth Science Fund. Han Li reports financial support was provided by Key Scientific Research Project of Henan Province Colleges and Universities. Han Li reports financial support was provided by Xinxiang Medical University Doctor Support Foundation. Jinghui Wei reports financial support was provided by Graduate Research Innovation Support Program. Xuejia Liu reports financial support was provided by Graduate Research Innovation Support Program. If there are other authors, they declare that they have no known competing financial interests or personal relationships that could have appeared to influence the work reported in this paper.

Acknowledgements

Not applicable.

Appendix A. Supplementary data

Supplementary data to this article can be found online at https://doi.org/10.1016/j.reth.2024.03.003.

References

[1] Hoang DM, Pham PT, Bach TQ, Ngo ATL, Nguyen QT, Phan TTK, et al. Stem cell-based therapy for human diseases. Signal Transduct Targeted Ther 2022;7:272. https://doi.org/10.1038/s41392-022-01134-4.

[2] Li H, Wei J, Liu X, Zhang P, Lin J. Muse cells: ushering in a new era of stem cell-based therapy for stroke. Stem Cell Res Ther 2022;13:421. https://doi.org/10.1186/s13287-022-03126-1.

[3] Tamai K, Yamazaki T, Chino T, Ishii M, Otsuru S, Kikuchi Y, et al. PDGFRalpha-positive cells in bone marrow are mobilized by high mobility group box 1 (HMGB1) to regenerate injured epithelia. Proc Natl Acad Sci USA 2011;108:6609–14. https://doi.org/10.1073/pnas.1016753108.

[4] Wolff EF, Mutlu L, Massasa EE, Elsworth JD, Eugene Redmond D, Taylor HS. Endometrial stem cell transplantation in MPTP- exposed primates: an alternative cell source for treatment of Parkinson's disease. J Cell Mol Med 2015;19:249–56. https://doi.org/10.1111/jcmm.12433.

[5] Iseki M, Kushida Y, Wakao S, Akimoto T, Mizuma M, Motoi F, et al. Muse cells, nontumorigenic pluripotent-like stem cells, have liver regeneration capacity through specific homing and cell replacement in a mouse model of liver

fibrosis. Cell Transplant 2017;26:821–40. https://doi.org/10.3727/096368916X693662.
[6] Bang OY, Lee JS, Lee PH, Lee G. Autologous mesenchymal stem cell transplantation in stroke patients. Ann Neurol 2005;57:874–82. https://doi.org/10.1002/ana.20501.
[7] Park YJ, Niizuma K, Mokin M, Dezawa M, Borlongan CV. Cell-based therapy for stroke: musing with Muse cells. Stroke 2020;51:2854–62. https://doi.org/10.1161/STROKEAHA.120.030618.
[8] Kuroda Y, Kitada M, Wakao S, Nishikawa K, Tanimura Y, Makinoshima H, et al. Unique multipotent cells in adult human mesenchymal cell populations. Proc Natl Acad Sci U S A 2010;107:8639–43. https://doi.org/10.1073/pnas.0911647107.
[9] Kuroda Y, Wakao S, Kitada M, Murakami T, Nojima M, Dezawa M. Isolation, culture and evaluation of multilineage-differentiating stress-enduring (Muse) cells. Nat Protoc 2013;8:1391–415. https://doi.org/10.1038/nprot.2013.076.
[10] Tanaka T, Nishigaki K, Minatoguchi S, Nawa T, Yamada Y, Kanamori H, et al. Mobilized muse cells after acute myocardial infarction predict cardiac function and remodeling in the chronic phase. Circ J 2018;82:561–71. https://doi.org/10.1253/circj.CJ-17-0552.
[11] Leng Z, Sun D, Huang Z, Tadmori I, Chiang N, Kethidi N, et al. Quantitative analysis of SSEA3+ cells from human umbilical cord after magnetic sorting. Cell Transplant 2019;28:907–23. https://doi.org/10.1177/0963689719844260.
[12] Heneidi S, Simerman AA, Keller E, Singh P, Li X, Dumesic DA, et al. Awakened by cellular stress: isolation and characterization of a novel population of pluripotent stem cells derived from human adipose tissue. PLoS One 2013;8:e64752. https://doi.org/10.1371/journal.pone.0064752.
[13] Ogura F, Wakao S, Kuroda Y, Tsuchiyama K, Bagheri M, Heneidi S, et al. Human adipose tissue possesses a unique population of pluripotent stem cells with nontumorigenic and low telomerase activities: potential implications in regenerative medicine. Stem Cell Dev 2014;23:717–28. https://doi.org/10.1089/scd.2013.0473.
[14] Gimeno ML, Fuertes F, Barcala Tabarrozzi AE, Attorressi AI, Cucchiani R, Corrales L, et al. Pluripotent nontumorigenic adipose tissue-derived muse cells have immunomodulatory capacity mediated by transforming growth factor-β1. Stem Cells Trans Med 2017;6:161–73. https://doi.org/10.5966/sctm.2016-0014.
[15] Liu Q, Zhang RZ, Li D, Cheng S, Yang YH, Tian T, et al. Muse cells, a new type of pluripotent stem cell derived from human fibroblasts. Cell Reprogr 2016;18:67–77. https://doi.org/10.1089/cell.2015.0085.
[16] Kushida Y, Wakao S, Dezawa M. Muse cells are endogenous reparative stem cells. Adv Exp Med Biol 2018;1103:43–68. https://doi.org/10.1007/978-4-431-56847-6_3.
[17] Meng X, Ichim TE, Zhong J, Rogers A, Yin Z, Jackson J, et al. Endometrial regenerative cells: a novel stem cell population. J Transl Med 2007;5:57. https://doi.org/10.1186/1479-5876-5-57.
[18] Cui C-H, Uyama T, Miyado K, Terai M, Kyo S, Kiyono T, et al. Menstrual blood-derived cells confer human dystrophin expression in the murine model of Duchenne muscular dystrophy via cell fusion and myogenic transdifferentiation. Mol Biol Cell 2007;18:1586–94. https://doi.org/10.1091/mbc.e06-09-0872.
[19] Li H, Yahaya BH, Ng WH, Yusoff NM, Lin J. Conditioned medium of human menstrual blood-derived endometrial stem cells protects against MPP(+)-induced cytotoxicity in vitro. Front Mol Neurosci 2019;12:80. https://doi.org/10.3389/fnmol.2019.00080.
[20] Dominici M, Le Blanc K, Mueller I, Slaper-Cortenbach I, Marini F, Krause D, et al. Minimal criteria for defining multipotent mesenchymal stromal cells. The International Society for Cellular Therapy position statement. Cytotherapy 2006;8:315–7. https://doi.org/10.1080/14653240600855905.
[21] Paxinos GWC. The rat brain in stereotaxic coordinates. CA: Academic Press; 2007.
[22] Chen J, Li Y, Wang L, Zhang Z, Lu D, Lu M, et al. Therapeutic benefit of intravenous administration of bone marrow stromal cells after cerebral ischemia in rats. Stroke 2001;32:1005–11. https://doi.org/10.1161/01.str.32.4.1005.
[23] Uchida H, Morita T, Niizuma K, Kushida Y, Kuroda Y, Wakao S, et al. Transplantation of unique subpopulation of fibroblasts, muse cells, ameliorates experimental stroke possibly via robust neuronal differentiation. Stem Cell 2016;34:160–73. https://doi.org/10.1002/stem.2206.
[24] Yamashita T, Kushida Y, Wakao S, Tadokoro K, Nomura E, Omote Y, et al. Therapeutic benefit of Muse cells in a mouse model of amyotrophic lateral sclerosis. Sci Rep 2020;10:17102. https://doi.org/10.1038/s41598-020-74216-4.
[25] Nitobe Y, Nagaoki T, Kumagai G, Sasaki A, Liu X, Fujita T, et al. Neurotrophic factor secretion and neural differentiation potential of multilineage-differentiating stress-enduring (Muse) cells derived from mouse adipose tissue. Cell Transplant 2019;28:1132–9. https://doi.org/10.1177/0963689719863809.
[26] Kinoshita K, Kuno S, Ishimine H, Aoi N, Mineda K, Kato H, et al. Therapeutic potential of adipose-derived SSEA-3-positive muse cells for treating diabetic skin ulcers. Stem Cells Transl Med 2015;4:146–55. https://doi.org/10.5966/sctm.2014-0181.
[27] Aprile D, Alessio N, Squillaro T, Di Bernardo G, Peluso G, Galderisi U. Role of glycosphingolipid SSEA-3 and FGF2 in the stemness and lineage commitment of multilineage differentiating stress enduring (MUSE) cells. Cell Prolif 2023;56:e13345. https://doi.org/10.1111/cpr.13345.
[28] Yin XY, Wang CC, Du P, Wang XS, Lu YC, Sun YW, et al. Muse cells decrease the neuroinflammatory response by modulating the proportion of M1 and M2 microglia in vitro. Neural Regen Res 2023;18:213–8. https://doi.org/10.4103/1673-5374.343885.
[29] Mao XQ, Cheng Y, Zhang RZ, Liu YB, Li Y, Ge K, et al. RNA-seq and ATAC-seq analyses of multilineage differentiating stress enduring cells: comparison with dermal fibroblasts. Cell Biol Int 2022;46:1480–94. https://doi.org/10.1002/cbin.11834.
[30] Fei W, Wu J, Gao M, Wang Q, Zhao YY, Shan C, et al. Multilineage-differentiating stress-enduring cells alleviate atopic dermatitis-associated behaviors in mice. Stem Cell Res Ther 2021;12:606. https://doi.org/10.1186/s13287-021-02671-5.
[31] Chen X, Yin XY, Zhao YY, Wang CC, Du P, Lu YC, et al. Human Muse cells-derived neural precursor cells as the novel seed cells for the repair of spinal cord injury. Biochem Biophys Res Commun 2021;568:103–9. https://doi.org/10.1016/j.bbrc.2021.06.070.
[32] Uchida H, Niizuma K, Kushida Y, Wakao S, Tominaga T, Borlongan CV, et al. Human muse cells reconstruct neuronal circuitry in subacute lacunar stroke model. Stroke 2017;48:428–35. https://doi.org/10.1161/strokeaha.116.014950.
[33] Wang P, Wang S, Ji F, Zhang R. Muse cells have higher stress tolerance than adipose stem cells due to the overexpression of the CCNA2 gene. Stem Cell Dev 2021;30:1056–69. https://doi.org/10.1089/scd.2021.0088.
[34] Lanctot PM, Gage FH, Varki AP. The glycans of stem cells. Curr Opin Chem Biol 2007;11:373–80. https://doi.org/10.1016/j.cbpa.2007.05.032.
[35] Pan S, Chen W, Liu X, Xiao J, Wang Y, Liu J, et al. Application of a novel population of multipotent stem cells derived from skin fibroblasts as donor cells in bovine SCNT. PLoS One 2015;10:e0114423. https://doi.org/10.1371/journal.pone.0114423.
[36] Yamada Y, Wakao S, Kushida Y, Minatoguchi S, Mikami A, Higashi K, et al. S1P-S1PR2 axis mediates homing of Muse cells into damaged heart for long-lasting tissue repair and functional recovery after acute myocardial infarction. Circ Res 2018;122:1069–83. https://doi.org/10.1161/CIRCRESAHA.117.311648.
[37] Wakao S, Kitada M, Kuroda Y, Shigemoto T, Matsuse D, Akashi H, et al. Multilineage-differentiating stress-enduring (Muse) cells are a primary source of induced pluripotent stem cells in human fibroblasts. Proc Natl Acad Sci U S A 2011;108:9875–80. https://doi.org/10.1073/pnas.1100816108.
[38] Verstockt B, Vetrano S, Salas A, Nayeri S, Duijvestein M, Vande Casteele N. Sphingosine 1-phosphate modulation and immune cell trafficking in inflammatory bowel disease. Nat Rev Gastroenterol Hepatol 2022;19:351–66. https://doi.org/10.1038/s41575-021-00574-7.
[39] McGinley MP, Cohen JA. Sphingosine 1-phosphate receptor modulators in multiple sclerosis and other conditions. Lancet (London, England) 2021;398:1184–94. https://doi.org/10.1016/s0140-6736(21)00244-0.
[40] Oguma Y, Kuroda Y, Wakao S, Kushida Y, Dezawa M. Single-cell RNA sequencing reveals different signatures of mesenchymal stromal cell pluripotent-like and multipotent populations. iScience 2022;25:105395. https://doi.org/10.1016/j.isci.2022.105395.
[41] Alessio N, Squillaro T, Özcan S, Di Bernardo G, Venditti M, Melone M, et al. Stress and stem cells: adult Muse cells tolerate extensive genotoxic stimuli better than mesenchymal stromal cells. Oncotarget 2018;9:19328–41. https://doi.org/10.18632/oncotarget.25039.
[42] Fu H, Subramanian RR, Masters SC. 14-3-3 proteins: structure, function, and regulation. Annu Rev Pharmacol Toxicol 2000;40:617–47. https://doi.org/10.1146/annurev.pharmtox.40.1.617.
[43] Mhawech P. 14-3-3 proteins–an update. Cell Res 2005;15:228–36. https://doi.org/10.1038/sj.cr.7290291.
[44] Gardino AK, Yaffe MB. 14-3-3 proteins as signaling integration points for cell cycle control and apoptosis. Semin Cell Dev Biol 2011;22:688–95. https://doi.org/10.1016/j.semcdb.2011.09.008.